ELSEVIER

Journal of Contaminant Hydrology 38 (1999) 185–215

JOURNAL OF
Contaminant
Hydrology

A site-scale model for fluid and heat flow in the unsaturated zone of Yucca Mountain, Nevada

Yu-Shu Wu *, Charles Haukwa, G.S. Bodvarsson

Earth Sciences Division, E.O. Lawrence Berkeley National Laboratory, Berkeley, CA 94720, USA

Accepted 29 October 1998

Abstract

A three-dimensional unsaturated-zone numerical model has been developed to simulate flow and distribution of moisture, gas and heat at Yucca Mountain, Nevada, a potential repository site for high-level radioactive waste. The model takes into account the simultaneous flow dynamics of liquid water, vapor, air and heat in the highly heterogeneous, fractured porous rock in the unsaturated zone (UZ). This model is intended for use in the prediction of the current and future conditions in the UZ so as to aid in the assessment of the system performance of the proposed repository. The modeling approach is based on a mathematical formulation of coupled multiphase, multicomponent fluid and heat flow through porous and fractured rock. Fracture and matrix flow is treated using both dual-permeability and effective-continuum modeling approaches. The model domain covers a total area of approximately 43 km^2, and uses the land surface and the water table as its top and bottom boundaries. In addition, site-specific data, representative surface infiltration, and geothermal conditions are incorporated into the model. The reliability and accuracy of the model have been the subject of a comprehensive model calibration study, in which the model was calibrated against measured data, including liquid saturation, water potential and temperature. It has been found that the model is generally able to reproduce the overall system behavior at Yucca Mountain with respect to moisture profiles, pneumatic pressure variations in different geological units, and ambient geothermal conditions.

Keywords: Numerical reservoir simulation; Unsaturated zone; Yucca Mountain; Site-scale numerical model; Multiphase flow; Heat transfer

1. Introduction

Quantitative evaluation of moisture, gas, and heat flow, and their effects on the performance of the potential high-level nuclear waste repository at Yucca Mountain is

* Corresponding author. Fax: +1-510-486-6115; e-mail: yswu@lbl.gov

PII: S0169-7722(99)00014-5

essential for conducting site characterization studies, and for designing the repository and engineered barrier system. Numerical modeling has played a crucial role in understanding unsaturated-zone (UZ) fluid movement, and the effects of hydrogeologic and thermal conditions on various aspects of the overall waste-disposal system. Whereas laboratory and field experiments are limited in space and time, numerical modeling provides a means to study physical processes on large temporal and spatial scales that are relevant to understanding of nuclear waste disposal in a geologic formation. Performance assessment models based on numerical simulation of water, gas and heat flow can include all known important physical and chemical processes that affect the behavior of the repository and the host rock.

A number of numerical models for evaluating the unsaturated-zone hydrologic conditions at Yucca Mountain have been developed since the 1980’s. Rulon et al. (1986) used two-dimensional cross-sectional models to investigate important flow processes at Yucca Mountain, including lateral flow within the Paintbrush unit and the effects of fracture and matrix flow. This work was followed by a number of studies of processes on a more basic level than site-scale coupled processes. Pollock (1986) developed a mathematical model for analyzing one-dimensional, vertical transport of energy, water and air in unsaturated alluvium. Tsang and Pruess (1987) studied thermally induced convection phenomena near a high-level nuclear waste repository in partially saturated tuffs using a two-dimensional model. One of the earlier studies of gas flow at Yucca Mountain was presented by Weeks (1987) to explain air circulation as observed from boreholes.

In the early 1990’s, Wittwer et al. (1992, 1995) started development of a three-dimensional (3D) model that incorporated many geological and hydrological complexities, such as geological layering, degree of welding, fault offsets, differing matrix and fracture properties, and others. Ahlers et al. (1995a,b) continued development of the UZ model with increased numerical and spatial resolution. Their studies considered processes such as gas pressures and moisture flow, temperature and heat-flow analyses, and rock-property evaluation through inverse modeling. A detailed comparison of the model predictions with measured data from the site was reported by Wu et al. (1996a, 1997).

Several similar models have also been developed that have enhanced the understanding of single- and coupled flow and transport processes within the UZ. Wang and Narasimhan (1987) showed that the degree of lateral flow at the Yucca Mountain site depends strongly on assumed hydrological parameters of vertical fault zones, especially their characteristic curves. Other work by Wang and Narasimhan (1985) suggested that effects of infiltration pulses at the surface are dampened by the underlying tuff units. Their results showed that the welded tuff of the potential repository horizon exhibited only small changes in saturations, pressures, and potentials from steady-state values in response to the transient pulses.

One of the first 3D models of Yucca Mountain was developed by Rockhold et al. (1990), who studied the UZ in the immediate vicinity of the potential repository, and found considerable lateral flow due to the complex stratigraphy. The various cases considered predicted mostly fracture-dominated flow in the shallow welded units (Tiva Canyon formation), but matrix-dominated flow elsewhere. Concurrent modeling work by Flint et al. (1993) was used to predict saturation and water potential profiles in boreholes drilled at the site. Arnold et al. (1995) used 2D cross-section models to evaluate the travel time of fluid from the proposed repository level to the water table. Ho (1994) evaluated flow into a welded tuff matrix material from a saturated vertical fracture. Robinson et al. (1995, 1996, 1997) presented the results of flow and transport modeling for various radioactive isotopes, along with sensitivity analyses using various infiltration scenarios.

The 3D UZ model presented in this paper is built on the analysis and the results of the above-referenced work and many other studies. The primary objective of the UZ model of Yucca Mountain is to develop a reliable computer model to simulate and investigate the existing natural state of the system, and predict possible future system responses. As a critical step of model development, a series of model calibrations and sensitivity analyses have been conducted with the 3D site-scale model to investigate effects of variations in rock and fault properties and in model boundary conditions, and various issues regarding different conceptual models.

Modeling coupled processes in large-scale, three-dimensional, fractured systems is conceptually difficult and computationally demanding. One key issue for simulating fluid and heat flow in the fractured welded units of the Yucca Mountain site is how to evaluate fracture and matrix interactions under multiphase, nonisothermal conditions. The available methods for treatment of fracture and porous matrix interactions rely generally on numerical approaches. These include: (1) explicit discrete fracture and matrix model; (2) the effective-continuum method (ECM); (3) the double- or multiporosity method (Wu and Pruess, 1988); (4) the dual-permeability method; and (5) the more general ‘multiple interacting continua’ (MINC) method (Pruess and Narasimhan, 1985). We have experimented with all of these options for treating fracture and matrix flow in our modeling studies at Yucca Mountain. When applied to simulating moisture flow and heat transfer at the mountain, all these approaches require knowledge of fracture and matrix properties and their spatial distribution. These site-specific fracture/matrix parameters, however, are presently not well defined for many hydrogeological units at Yucca Mountain.

Modeling approach used in this study employs large-scale spatial and temporal averaging in representing the heterogeneous fracture and matrix system at Yucca Mountain. This volume-averaged concept may not capture phenomena associated with ‘fast’ flow and solute transport along localized preferential pathways on a much smaller scale than grid block size. Evidence that water flow in thick UZs in fractured rocks may occur in non-volume averaged fashion is discussed by Pruess et al., 1999. They have also presented several alternative concepts and modeling approaches to address fast flow issues in unsaturated fractured rocks. Theoretically, it is possible to simulate those localized flow and transport processes using a volume averaged, continuum approach if sufficiently detailed spatial discretization is used. However, computation intensity and lack in detailed knowledge of fracture/matrix characterization make it impossible to exercise this effort to a realistic site application.

Currently, the effective-continuum approach has found wide applications, due to its simplicity in terms of data requirement and the computational efficiency in handling large model grids (Wu et al., 1996a,b). On the other hand, the dual-permeability approach is preferable because of its flexibility in handling matrix–fracture interaction, and matrix to matrix flow, which may be important for moisture movement within Yucca Mountain. For these reasons, both the ECM and dual-permeability modeling approaches are used in this paper to evaluate fracture–matrix flow. Comparison studies using the full 3D model grid under the same boundary and initial conditions (Wu et al., 1996a) showed that for steady-state moisture distributions and movement within the mountain, the ECM approach gives almost identical results to the dual-permeability model for a given site conceptual model. A similar conclusion was also obtained (Doughty and Bodvarsson, 1996, 1997, 1999, this issue) for transient gas flow and ambient heat transfer, in which the ECM model gives accurate results when compared with results from a dual-continua approach.

Numerous model simulations were performed to quantify the sensitivity of the model to the parameters and assumptions used in the model preparation. The emphases of the modeling efforts were to examine the accuracy and reliability of the model in predicting hydrogeological conditions at the mountain. The effects of rock property variation and heterogeneity were tested using rock property data from several available sets of parameters estimated by inverse modeling (Bandurraga and Bodvarsson, 1997). Other sensitivity studies related to model set-up and input parameters include the effects of boundary-condition uncertainty, surface net infiltration and fault representations. The results of these studies will be used to provide directions for future modeling, as well as field-data collection efforts.

The 3D model calibration studies of this paper indicate that the 3D site-scale UZ flow model can in general reproduce the moisture and geothermal conditions at Yucca Mountain. The moisture distributions predicted by the 3D model agree well with observed water-saturation profiles, and are in reasonable agreement with measured borehole water potentials. Simulated temperature profiles are in good agreement with observed temperatures at more than 20 boreholes. The capability of the UZ model to reproduce these conditions is critical to various Yucca Mountain site characterization project activities. The model provides a useful tool for evaluating alternative conceptual models of fracture/matrix flow, heat transfer and chemical transport within the mountain.

As examples of model applications, based on the confidence built through model calibration and sensitivity analyses, we present simulation results and predictions of: (1) ambient moisture and geothermal conditions of the repository site, and (2) percolation flux at the repository horizon.

2. Model description

The first paper of this issue (Bodvarsson et al., this issue) provide the basic background information on the Yucca Mountain site as well as an introduction to the unsaturated-zone model. Subsurface hydrologic processes at Yucca Mountain occur in a heterogeneous environment of layered, anisotropic, fractured volcanic rocks (Scott and Bonk, 1984; Rousseau et al., 1996). These volcanics consist of alternating layers of welded and nonwelded ash flow and air fall tuffs. The primary geologic formations found at Yucca Mountain, beginning from the land surface, consist of the Tiva Canyon, Yucca Mountain, Pah Canyon, and the Topopah Spring Tuffs of the Paintbrush Group.

Underlying these are the Calico Hills Formation, and the Prow Pass, Bullfrog, and Tram Tuffs of the Crater Flat Group (Buesch et al., 1995). Table 1 lists the geological units for different hydrogeologic units and the associated model numerical grid layer information.

Table 1
The relations of geological and hydrogeological units, formation and model grid layers used in the 3D site-scale model

Geological unit	Welding intensity / Formation name (Buesch et al., 1995)	Model grid layer name	Hydrogeological unit
Paintbrush Group			
Tiva Canyon	M,D[a] (Tpcxxxx)	tcw11, tcw12	Tiva Canyon (TCw)
Tuff	D-Basal Vitrophyre (Tpcpv3), M (Tpcpv2)	tcw13	
	N,P (Tpcpv1)	ptn21	
Bedded tuff	N (Tpbt4)		Paintbrush (PTn)
Yucca Mountain Tuff	N,P,M (Tpy)	ptn22	
Bedded tuff	N (Tpbt3)	ptn23	
Pah Canyon Tuff	N,P,M (Tpy)	ptn24	
Bedded tuff	N (Tpbt2)		
Topopah Spring Tuff	N,P (Tptrv3)	ptn25	
	M (Tptrv2)	tsw31	Topopah Spring (TSw)
	D-Upper vitrophyre (Tptrv1)		
	M,D (Tptrn)	tsw32	
	M,D,L (Tptrl)		
	M,D,L (Tptpul)	tsw33	
	D (Tptpmn)	tsw34	
	M,D,L (Tptpll)	tsw35	
	D (Tptpln)	tsw36	
	D (Tptpv3)	tsw37	
	N,P,M; may be altered (Tptpv1, Tptpv2)		Calico Hills (CHn)
Bedded tuff	N; may be altered (Tpbt1)	ch1zc ch1vc	
Calico Hills Formation	N; unaltered (Ta-Vitric)	ch2vc	
	N; altered (Ta-Zeolitic)	ch3zc	
	N; may be altered (Tabt1)	ch4zc ch4vc	
Crater Flat Group			
Prow Pass Tuff	N; may be altered (Tpc) Unit 4[c]		
	N,P,M Unit 3	pp3vp	
	N,P; generally altered Units 2,1	pp2zp	
Bedded tuff	N; generally altered (Tpcbt1)		
Upper Bullfrog Tuff	N,P; generally altered (Tcb)		
Middle Bullfrog Tuff	N,P,M	bf3vp	
Lower Bullfrog Tuff	N,P; generally altered	bf2zp	Crater Flat undifferentiated (CFu)
Bedded tuff	N; generally altered (Tcbbt)		
Upper Tram Tuff	N,P; generally altered (Tct)	tm3vt	

[a]Welding intensity N = Non-; P = Partially; M = Moderately; D = Densely.
[b]L = Lithophysal Zone.
[c]Units per Moyer and Geslin (Buesch et al., 1995).

These geologic formations have been reorganized into hydrogeologic units based roughly on the degree of welding (Montazer and Wilson, 1984). These are the Tiva Canyon welded (TCw) hydrogeologic unit, the Paintbrush nonwelded unit (PTn), consisting primarily of the Yucca Mountain and Pah Canyon members and their bedded tuffs, the Topopah Spring welded (TSw) unit, the Calico Hills nonwelded (CHn), and the Crater Flat undifferentiated (CFu) units.

In addition to the highly heterogeneous and anisotropic nature of the fractured tuffs existing at the mountain, moisture flow is complicated by numerous strike–slip and normal faults with varying amounts of offset (Scott and Bonk, 1984). The vertical offset along these faults commonly ranges from ten to hundreds of meters, and generally increases from north to south. In the repository area the Ghost Dance fault has offsets of tens of meters (Spengler et al., 1993), while the Solitario Canyon fault located to the west has offsets of up to several hundreds of meters. These and other major faults may penetrate the complete thickness of the UZ, and control moisture flow and saturation distributions.

Under natural hydrological and geothermal conditions, both liquid and gas (air and vapor) flow in the UZ of the mountain are affected by ambient temperature changes, geothermal gradients, atmospheric and water table conditions. Thermal and hydrological regimes are closely related by the effects of coupling of thermal, density, and atmospheric conditions on air circulation through the mountain (Weeks, 1987; Lu and Kwicklis, 1995). In addition to the ambient thermal conditions, heat will be generated as a result of emplacing high-level nuclear waste in the UZ. Thermal loading from the waste repository will significantly affect the post-waste emplacement performance of the repository, and will create complex multiphase fluid flow and heat transfer processes (Wu et al., 1995). The physical mechanisms include, but are not limited to, conductive and convective heat transfer, phase change (vaporization and condensation), flow of liquid and gas under variably saturated conditions, and diffusion and dispersion of vapor and air. The result is that thermal effects must be included for accurate modeling of post-waste emplacement moisture flow through the mountain.

2.1. Model domain and grid

The 3D model domain and the numerical grid for this study are shown in plan view in Fig. 1. The model domain covers a total area of approximately 43 km^2, roughly from 2 km north of borehole G-2 in the north, to borehole G-3 in the south, and from the Bow Ridge fault in the east to about 1 km west of the Solitario Canyon fault. Fig. 1 shows the numerical grid with increased resolution (finer mesh), in the vicinity of the proposed repository, located near the center of the model domain. Also, shown in Fig. 1 are the locations of several of the boreholes used for model calibration. The model domain was selected to focus our study at and near the potential repository area, and to investigate effects of the major faults on moisture flow around the repository. All the laterally surrounding boundaries are located sufficiently far from the repository so that their effects on the simulation results at the repository are small.

In the vertical direction, the layering and subdivision of geological units in the numerical grid are based on the geological model of Bandurraga (1996). Fig. 2 shows

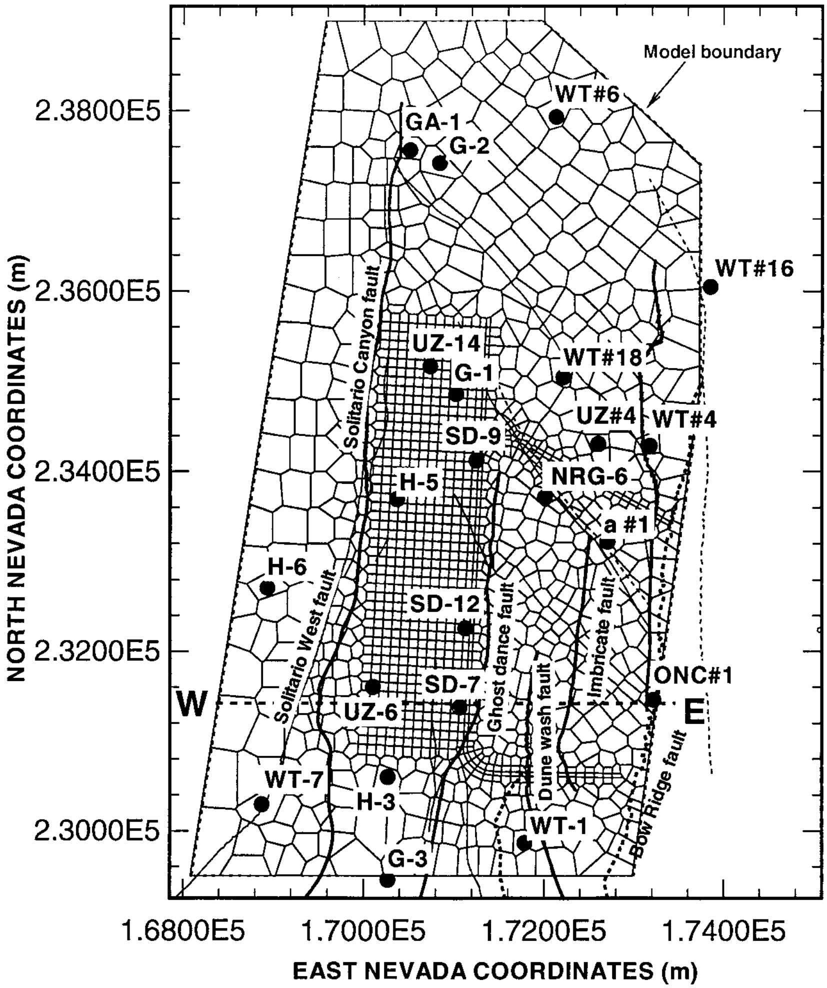

Fig. 1. Plan view of the 3D site-scale model domain, grid and incorporated major faults.

the vertical hydrogeological layers, and offsets of the explicitly modeled faults, along the cross section W–E of Fig. 1. The 3D model grid has 28 computational grid layers that represent different hydrogeological units and layers in the UZ of Yucca Mountain. From the top boundary (first layer) down, the Tiva Canyon unit (TCw) is vertically subdivided into three layers, although some are eroded and not present at all locations. The Paintbrush unit (PTn) is represented by five grid layers. Similarly to the TCw, several layers in the PTn are missing in areas of the site. The Topopah Spring (TSw) is divided into seven sublayers, with an additional three layers representing the repository area. The Calico Hills (CHn) has a maximum of eight sublayers, but because of lateral variation in the degree of zeolitization, generally about five layers are present in most locations. The bottom boundary of the model is at the water table.

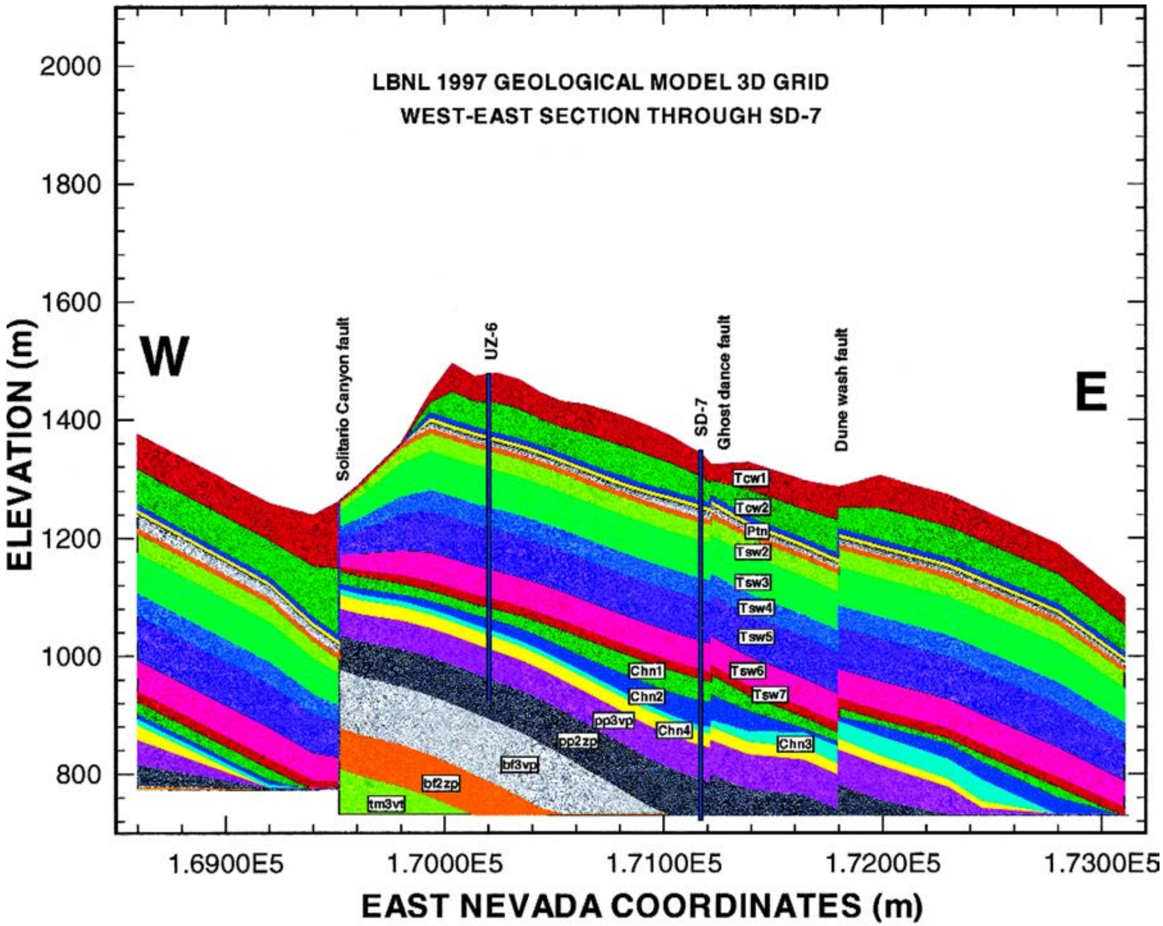

Fig. 2. West–East vertical cross section through the 3D model showing hydrogeological layers and offsets on the explicitly modeled faults.

Each 3D model grid layer has 1470 element blocks, leading to 1470 vertical grid columns for an ECM model. The ECM grid has a total number of 40,000 element blocks, and a total number of 140,000 connections between the blocks. The 3D grid was generated employing a Voronoi-type mesh. A Voronoi block is a region of space that is closer to a grid point than to any other point in the same plane. This method of mesh discretization fulfills the integral finite difference method formulation for flow calculation employed by the TOUGH2 code (Pruess, 1991), and ensures that all interface connections in the plane are perpendicular to the flow directions between connected blocks.

The dual-permeability grid is generated based on the ECM grid (Fig. 1) and the estimated properties of fractures (Sonnenthal et al., 1997). The conceptual model for fracture networks in the dual-permeability grid generation consists of fractures that are assumed to be parallel vertical plates with differences in apertures, spacings, and frequencies for different model layers, representing explicit geologic formations. The vertical parallel plate assumption is used because vertical fractures are predominant in most units, and connections between rock units are contributed mainly by vertical fractures, as observed from the underground tunnel and boreholes (Sonnenthal et al., 1997). The dual-permeability mesh subdivides each ECM element into fracture and matrix domains, doubling the number of total element blocks used in the ECM grid. The total number of connections in the dual-permeability grid then becomes 320,000.

It is a challenge to generate 3D numerical grids that model three-dimensional faults in a heterogeneous system. As shown in Figs. 1 and 2, several major faults are incorporated explicitly in the model, including the Solitario Canyon, Iron Ridge, Ghost Dance, Abandoned Wash, and Dune Wash faults. The Bow Ridge fault is treated as a boundary along the eastern edge of the model domain. Based on field evidence that the fault zones are dominantly vertical or near vertical at Yucca Mountain, the faults are represented in the model as vertical zones of finite thickness with sudden stratigraphic offset in connections to adjacent gridlayers. The scheme used for generating the fault grid elements is outlined by Wittwer et al. (1995).

2.2. Modeling approach

The simulation results presented here were carried out using the TOUGH2 code, a general-purpose reservoir simulator for simulating multidimensional coupled fluid and heat flow of multiphase, multicomponent fluid mixtures in porous and fractured media. In simulating thermohydrologic conditions in a high-level nuclear waste repository, two phases (liquid and gas), two components (water and air), and heat are considered in the TOUGH2 formulation (Pruess et al., 1990a,Pruess, 1991). The liquid phase contains a mixture of water and dissolved air, while the gas phase consists of water vapor and air. The flow of both liquid and gas phases is described by the multiphase extension of Darcy’s law, incorporating the effects of phase pressure, viscous, gravity, and capillary forces. Diffusive mass transport by binary diffusion of the air and vapor in the gas phase is included as an additional transport mechanism; however, liquid phase diffusion and hydrodynamic dispersive fluxes of the individual components are neglected. Heat transfer is governed mainly by conduction and convection. Phase changes of vaporization and condensation are also included. The conservation of mass and energy gives rise to three governing equations for the two mass components (air and water) and heat.

The numerical approach of TOUGH2 is based on the integral finite difference method. The three conservation equations are discretized in space using the 'integral finite difference' method (Narasimhan and Witherspoon, 1976). The integral finite difference discretization does not require any reference to a global system of coordinates, and thus offers the advantage of being applicable to regular or irregular geometries of gridding in one, two and three dimensions. The method also makes it possible, by means of simple preprocessing of geometric data, to implement double- and multiple-porosity, or dual-permeability methods for treatment of flow in fractured porous media. In the TOUGH2 formulation, time is discretized fully implicitly using a first-order backward finite difference scheme. The resulting discretized finite difference equations for mass and energy balances are nonlinear, and are solved simultaneously using the Newton/Raphson iterative scheme.

The numerical modeling approaches used in this study for treatment of fracture/matrix flow include both the ECM method (Pruess et al., 1990b; Wu et al., 1996b) and the more rigorous dual-permeability approach (Pruess, 1991). The ECM method can accommodate two-phase flow in a fracture/matrix system, based on approximate thermodynamic equilibrium (locally) between fracture and matrix all the times. For two-phase flow in a fractured porous medium, the condition of local thermodynamic equilibrium requires that temperatures, phase pressures, densities and viscosities in fracture and matrix systems are the same. Addition of the fluxes from Darcy's law for fracture and matrix gives the expressions for total flux through the fracture and matrix system:

$$F_\beta = -kk_\beta \frac{\rho_\beta}{\mu_\beta}\left(\nabla P_\beta - \rho_\beta g\right) \tag{1}$$

where $\boldsymbol{F}_\beta$ is the total mass flux vector for phase β; β is phase index (β = l for liquid, and β = g for gas); ρ_β is the density of phase β; μ_β is the viscosity of phase β; P_β is the pressure of phase β; and g is the acceleration of gravity. In Eq. (1), k is the effective-continuum permeability, defined as

$$k = k_\mathrm{m} + k_\mathrm{f} \tag{2}$$

with k_m being intrinsic continuum matrix permeability and k_f intrinsic continuum fracture permeability. The effective-continuum relative permeability, k_β, can be defined as

$$k_\beta = \frac{k_\mathrm{m} k_{\beta,\mathrm{m}} + k_\mathrm{f} k_{\beta,\mathrm{f}}}{k_\mathrm{m} + k_\mathrm{f}} \tag{3}$$

where $k_{\beta,\mathrm{m}}$ and $k_{\beta,\mathrm{f}}$ are relative permeability to phase β in matrix and fracture, respectively. In these equations we have defined relative permeabilities relative to the total single phase permeability, so that $0 < k_\beta < 1$. The expression for the total flux of Eq. (1) can be interpreted as referring to a single effective continuum with total effective phase permeability of $k_\mathrm{m}\ k_{\beta,\mathrm{m}} + k_\mathrm{f}\ k_{\beta,\mathrm{f}}$.

The ECM method, when applicable, provides a substantial simplification in the description of fluid and heat flow in fractured porous media, with a commensurate decrease in computational effort. Conditions are favorable for this method when rock matrix blocks are relatively small and permeable, and the fracture network is relatively uniformly distributed. The ECM formulation will be particularly suitable for a situation when a long-term, averaged, or steady-state solution is being sought (Pruess et al., 1990a,b). The effective-continuum approximation may break down under certain unfavorable conditions, such as very tight, large and low permeability rock matrix blocks with rapid transients through surrounding fractures, as it may take a long time to reach equilibrium under such conditions (Wu and Pruess, 1988).

At Yucca Mountain, the averaged net water-infiltration rate into the UZ has been estimated to be low, on the order of 5 mm/year. At most, infiltration rates may be as high as 20 mm/year in certain areas of the mountain (Hudson and Flint, 1995; Flint et al., 1996). The percolation water flux through the mountain is therefore expected to be small in most locations. Under these conditions local hydraulic equilibrium between porous rock matrix and fractures may be a reasonable approximation, and the ECM formulation may provide reasonable simulation results for predicting steady-state fluid movement under ambient hydrogeologic conditions.

Unlike the ECM method, the dual-continua approach (e.g., dual permeability) represents each grid block by a fracture block and one or more matrix blocks. If each fracture grid block is associated with only one matrix grid block, fracture–matrix flow must be approximated as quasi-steady (Warren and Root, 1963). On the other hand, if the rock matrix associated with a given fracture grid block is discretized into multiple grid blocks, transient fracture–matrix flow can be simulated. If global flow occurs only between fracture grid blocks, the model is known as a double-porosity model, because fracture permeability alone controls large-scale, global flow, while the matrix contributes an additional sink or source term. If global flow occurs within both fracture and matrix continua, the model is known as a dual-permeability model (Pruess, 1991). Since matrix–matrix flow is considered to be important in moisture movement in the UZ of Yucca Mountain, the dual-permeability approach was used as a main modeling approach in this study.

2.3. Model boundary conditions

The ground surface of the mountain (or the tuff–alluvium contact, in areas of significant alluvial cover) is taken as the top model boundary, and the water table is treated as the bottom boundary. Both top and bottom boundaries of the model are treated as Dirichlet-type boundaries, i.e., constant (but spatially distributed) temperatures, gas pressures and liquid saturations are specified along these boundary surfaces. The surface infiltration is treated as source terms to the grid blocks in the second grid layer from the top, because the first layer is treated as a Dirichlet-type boundary with constant pressure and temperature to represent the atmospheric conditions.

All the lateral boundaries, as shown in Fig. 1, are treated as no-flow, or closed boundaries. This treatment should be reasonable for the eastern boundary, which is along the Bow Ridge fault, since high vertical permeability and lower capillary forces are expected for the fault. For the southern, western, and northern, lateral boundaries, no-flow boundaries may have little effects on moisture flow within and near the potential repository areas, since these boundaries are far away from the repository.

The constant temperatures on the top and bottom boundaries were based on field observation. Temperatures at the water table were interpolated from borehole temperature measurement data as reported by Sass et al. (1988). The water-table temperature values are generally higher in the southern part, and lower in the northern part of the model domain. The highest temperatures are near the southwest corner, and the lowest are in the north, near borehole G-2. The temperature map of the water table is consistent with that of Fridrich et al. (1994), with an average value of about 32°C.

Variation of land-surface temperature as a function of elevation was achieved using temperature data from two boreholes USW NRG-6 and NRG-7a, which had over a year continuous temperature-monitoring data (Rousseau, 1996), and represented by the following equation (Lu and Kwicklis, 1995):

$$T_a = T_{ref} + \lambda(Z_{ref} - Z) \tag{4}$$

where T_a is ground surface temperature at elevation Z, T_{ref} is temperature at reference elevation Z_{ref}, and λ is the atmospheric lapse rate (°C/m).

The annually averaged ground temperature at NRG-6 is 18.23°C, and at NRG-7a, it is 17.78°C (Rousseau, 1996). Using the surface-elevation data and the annually averaged temperatures at the two boreholes, we can calculate the atmospheric lapse rate, $\lambda \approx 0.01$°C/m at Yucca Mountain. Then the surface temperatures are determined using Eq. (4) and elevations of the top model meshes. The resulting surface temperatures show relatively lower temperatures in the northern part of the site, and along the ridge of the mountain, where higher elevations exist. In the remainder of the model domain, an average temperature is about 16° to 18°C.

The pressure conditions at the bottom boundary of the model are calculated using observed gas pressure values (Ahlers et al., 1995a,b, 1998). The water table, as the bottom boundary of the site-scale model, is a relatively flat, stable surface. In the eastern part of the site to the Solitario Canyon fault the water-table elevation is about 730 m above sea level (masl); however, the water-table elevation increases by 40 m when it crosses the Solitario Canyon fault to the west. The gas pressures are estimated using a pressure value of 0.92 bar at an elevation of 730 m. All the gas-pressure values of the bottom boundary elements are then calculated using elevations relative to the 730-m elevation for each boundary grid block, assuming that vapor-static conditions exist.

Surface gas pressures are determined by running the TOUGH2 code to steady-state under given temperature, bottom pressure, and surface infiltration conditions. This is necessary to generate a steady-state, equilibrated gas pressure boundary to avoid artificial air flow or circulation, which may happen when nonequilibrated pressures are imposed on the ground surface boundaries.

2.4. Infiltration

Infiltration, or net water recharge, through the top-soil layer of the mountain is the most important factor affecting the overall hydrological and thermohydrologic behavior of the UZ. Net infiltration is the ultimate source of groundwater recharge and percolation through the UZ, and provides the water for transport of radionuclides from the repository to the water table. Net infiltration at Yucca Mountain is spatially highly variable because of variations in soil cover and precipitation (Flint and Flint, 1994; Hudson and Flint, 1995). Although substantial research efforts have been devoted to determination of net infiltration over the mountain, direct measurements have proven difficult due to the low moisture flux and high potential evapotranspiration rates at the mountain area.

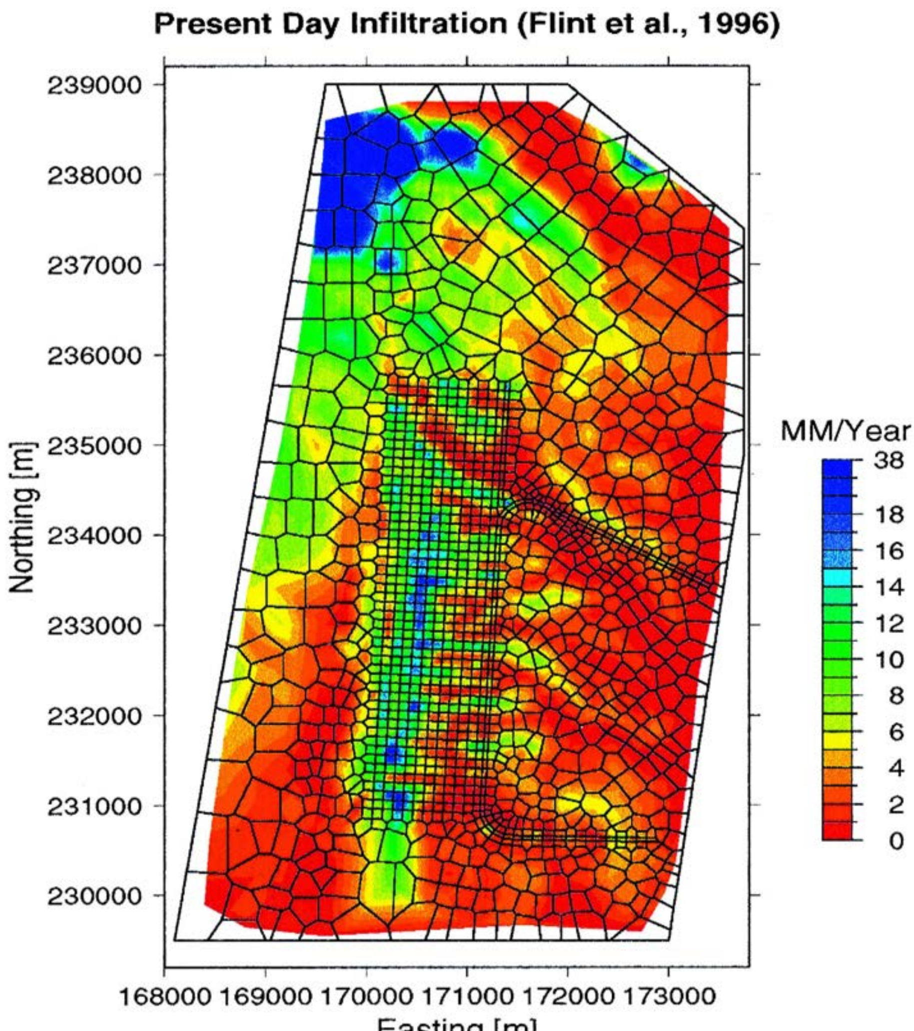

Fig. 3. Net infiltration map showing infiltration rates and spatial variations over the model domain of Yucca Mountain (Flint et al., 1996).

Most efforts to estimate net infiltration at the site have been based on average annual precipitation using an indirect method, with results ranging between 0 to more than 20 mm/year. The spatially variable net infiltration at the site, as estimated by Flint and Flint (1994) ranged from 0.02 to 13.40 mm/year. Their estimation was based on hydraulic property measurements of the bedrock units close to the surface, their steady-state water content, and an assumed unit hydraulic gradient. In 1995, their work was extended to describe the spatial distribution of shallow infiltration at Yucca Mountain (Hudson and Flint, 1995). This study, based on the neutron moisture meter logs at 84 locations conducted over a 10-year period and a multiple linear regression model, gave a much higher net infiltration over a modeled area of 150 km^2, with an average of 21.6 mm/year.

A recent, updated infiltration map (Flint et al., 1996) is used in this study, as shown in Fig. 3. The figure shows the distributions of net infiltration with an average infiltration rate of 4.9 mm/year over the model domain. The spatial distributions of

Table 2
Rock properties parameter for matrix and fractures, used in the model calibration and sensitivity studies

Layer/ Name	k_m (m^2)	k_f (m^2)	α_m (Pa^{-1})	α_f (Pa^{-1})	m_m	m_f	ϕ_f	$F\phi_f$ (m^{-1})	Units
tcw11	0.540E−17	0.503E−11	0.117E−5	0.237E−4	0.399	0.476	2.33E−4	1.020	TCw
tcw22	0.540E−17	0.600E−11	0.140E−5	0.237E−4	0.411	0.499	2.99E−4	1.830	
tcw33	0.500E−16	0.240E−11	0.800E−6	0.816E−4	0.471	0.503	7.05E−5	1.270	
ptn21	0.370E−12	0.335E−12	0.171E−3	0.110E−2	0.194	0.492	4.84E−5	0.870	PTn
ptn22	0.330E−14	0.457E−12	0.371E−4	0.185E−2	0.361	0.492	4.83E−5	0.290	
ptn23	0.102E−11	0.302E−11	0.450E−3	0.345E−2	0.214	0.492	1.30e−4	0.290	
ptn24	0.104E−12	0.117E−12	0.400E−3	0.913E−3	0.331	0.492	6.94E−5	0.630	
ptn25	0.574E−12	0.500E−12	0.653E−3	0.111E−2	0.262	0.492	8.32E−5	0.650	
tsw31	0.236E−14	0.120E−11	0.968E−5	0.630E−4	0.283	0.487	8.92E−5	1.100	TSw
tsw32	0.776E−15	0.820E−12	0.630E−4	0.794E−4	0.236	0.433	1.29E−4	1.010	
tsw33	0.880E−16	0.106E−11	0.661E−5	0.453E−4	0.249	0.494	1.05E−4	0.690	
tsw34	0.802E−17	0.435E−12	0.104E−5	0.103E−4	0.326	0.472	1.24E−4	1.880	
tsw35	0.226E−16	0.856E−12	0.330E−5	0.466E−4	0.234	0.456	3.29E−4	1.810	
tsw36	0.752E−17	0.152E−11	0.128E−5	0.139E−4	0.416	0.543	3.99E−4	2.100	
tsw37	0.488E−16	0.372E−11	0.238E−5	0.401E−4	0.385	0.526	4.92E−4	2.880	
ch1vc	0.160E−11	0.174E−11	0.657E−4	0.118E−2	0.190	0.492	7.14E−5	0.420	CHn
ch2vc	0.254E−12	0.288E−12	0.738E−4	0.118E−2	0.224	0.492	7.14E−5	0.420	
ch3vc	0.254E−12	0.288E−12	0.738E−4	0.118E−2	0.224	0.492	7.14E−5	0.420	
ch4vc	0.254E−12	0.288E−12	0.738E−4	0.118E−2	0.224	0.492	7.14E−5	0.420	
ch1zc	0.252E−16	0.251E−13	0.172E−5	0.307E−4	0.364	0.492	1.10E−5	0.067	
ch2zc	0.451E−17	0.251E−13	0.394E−5	0.103E−3	0.225	0.490	1.10E−5	0.067	
ch3zc	0.451E−17	0.251E−13	0.394E−5	0.103E−3	0.225	0.490	1.10E−5	0.067	
ch4zc	0.840E−17	0.251E−13	0.126E−5	0.107E−4	0.475	0.492	1.10E−5	0.067	
pp3vp	0.590E−14	0.431E−12	0.177E−4	0.563E−3	0.309	0.477	7.14E−5	0.420	
pp2zp	0.940E−17	0.251E−13	0.179E−5	0.151E−4	0.311	0.487	1.10E−5	0.067	
bf3vp	0.590E−14	0.431E−12	0.177E−4	0.563E−3	0.309	0.477	7.14E−5	0.420	
bf2zp	0.940E−17	0.251E−13	0.179E−5	0.151E−4	0.311	0.487	1.10E−5	0.067	CFu
tm3vt	0.590E−14	0.431E−12	0.177E−4	0.563E−3	0.309	0.477	7.14E−5	0.420	

Table 3
The rock properties for faults used in the model calibration studies

Units	k_m (m^2)	k_f (m^2)	α_m (Pa^{-1})	α_f (Pa^{-1})	m_m	m_f	ϕ_f	$F\phi_f$ (m^{-1})
TCw	1.0E − 13	2.0E − 11	0.61E − 4	1.0E − 3	0.50	0.50	3.34E − 4	4.51
PTn	1.0E − 13	2.0E − 13	0.61E − 4	1.0E − 3	0.50	0.50	3.34E − 4	4.51
TSw	1.0E − 13	2.0E − 11	0.61E − 4	1.0E − 3	0.50	0.50	3.34E − 4	4.51
CHn	5.0E − 15	5.0E − 14	0.61E − 4	1.0E − 3	0.50	0.50	3.34E − 4	4.51

infiltration, in Fig. 3, indicate that there are higher recharge rates in the northern part of the model domain and along the mountain ridge from south to north.

2.5. Model parameters and rock properties

All the simulations presented were performed using the TOUGH2 code (Pruess, 1991). Thermophysical properties of liquid water and vapor in the code are internally generated within experimental accuracy from steam table equations (International Formulation Committee, 1967). Air is treated as an ideal gas, and additivity of partial pressures is assumed for air/vapor mixtures. Rock thermal conductivities and heat

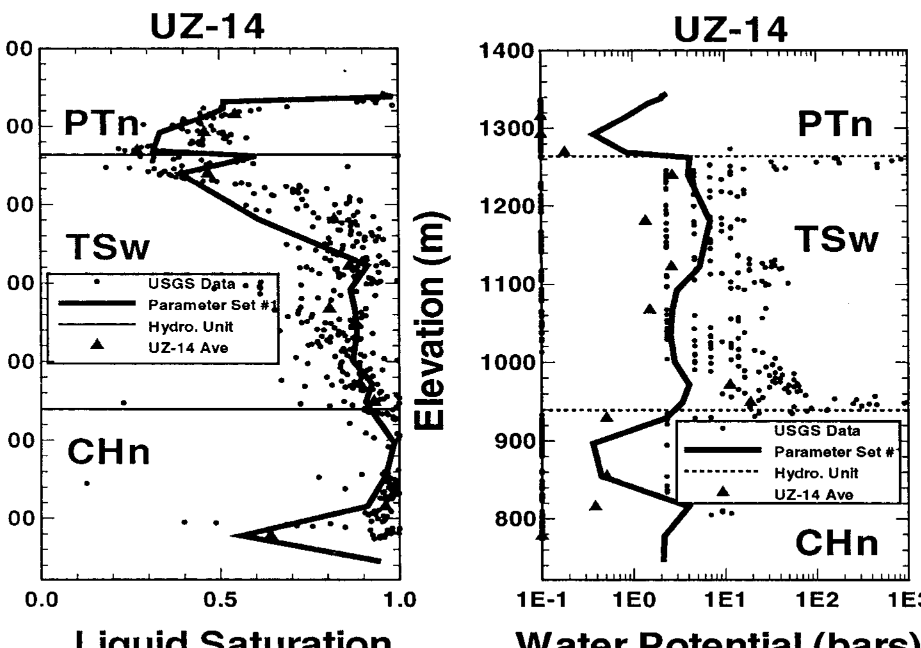

Fig. 4. Comparisons of the simulated and observed saturations and water potentials of borehole UZ-14.

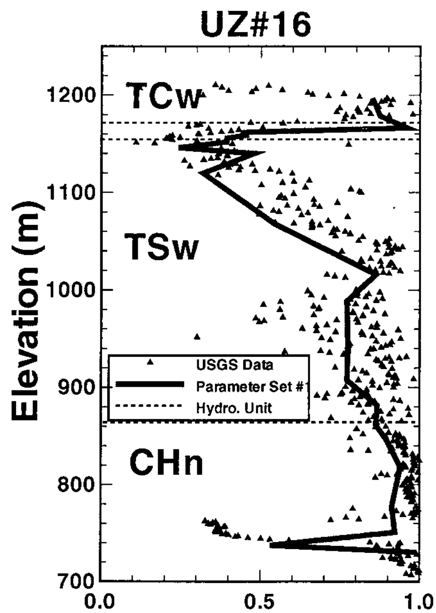

Fig. 5. Comparisons of the simulated and observed saturations of borehole UZ#16 (no measured water potential data available for this borehole).

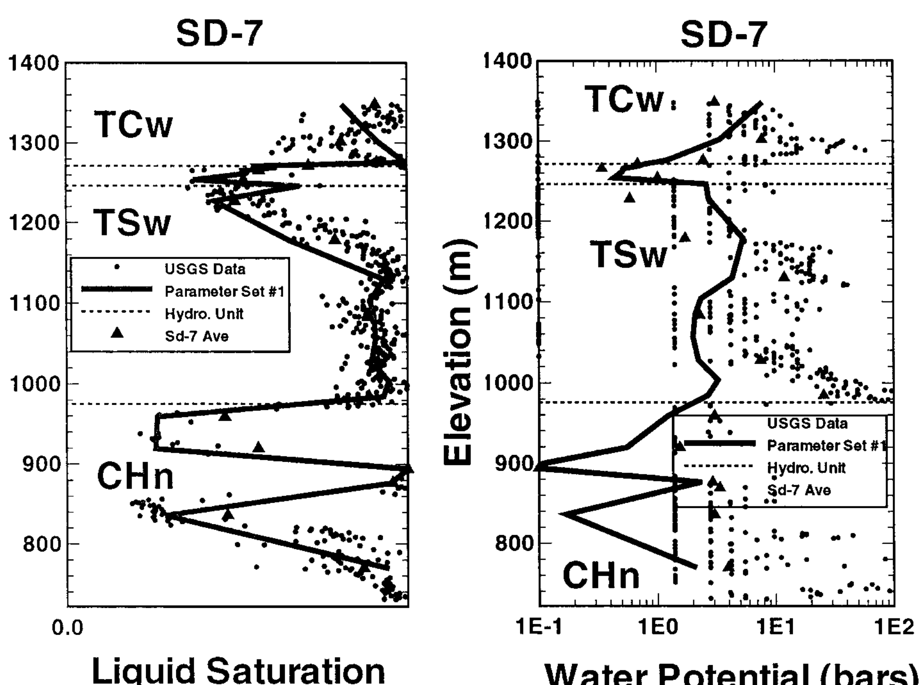

Fig. 6. Comparisons of the simulated and observed saturations and water potentials of borehole SD-7.

capacities used are from the Reference Information Base (RIB) (DOE, 1993) and Brodsky et al. (1997) for Yucca Mountain tuffs.

The rock properties used for matrix and fractures were estimated through inverse modeling and model calibrations, based on field and laboratory measurements of saturation and water potential data, pneumatic analysis and air permeability tests, and observed geochemical and fracture data (Bandurraga and Bodvarsson, 1997; Sonnenthal et al., 1997). The methodology and procedure of the parameter estimation were discussed by Bandurraga and Bodvarsson (1997), Bandurraga et al. (1996, 1999). In those parameter estimation studies, several sets of rock properties were obtained, due to inverse model input specification, conceptual models used, and alternative schemes for treating fracture–matrix interactions. One set of the rock properties estimated by the inverse study was chosen for use in this study because it was calibrated in the 3D modeling analysis (Wu et al., 1997), as given in Table 2.

The rock parameter specification in the 3D site-scale model is, in general, layer by layer, but certain grid layers in the CHn unit are altered to vitric or zeolitic regions. In these property-altered layers, zeolitic and vitric tuff properties are specified to correspond to geologic units and locations. The whole unsaturated-zone formation system is subdivided, in general, into 28 hydrogeological units or gridlayers, as discussed above. We treat all of the geological units as fracture/matrix systems, including fault zones.

In Table 2, α_m and α_f are van Genuchten's parameter (van Genuchten, 1980) of capillary pressure for matrix and fractures; m_m and m_f are van Genuchten's parameter

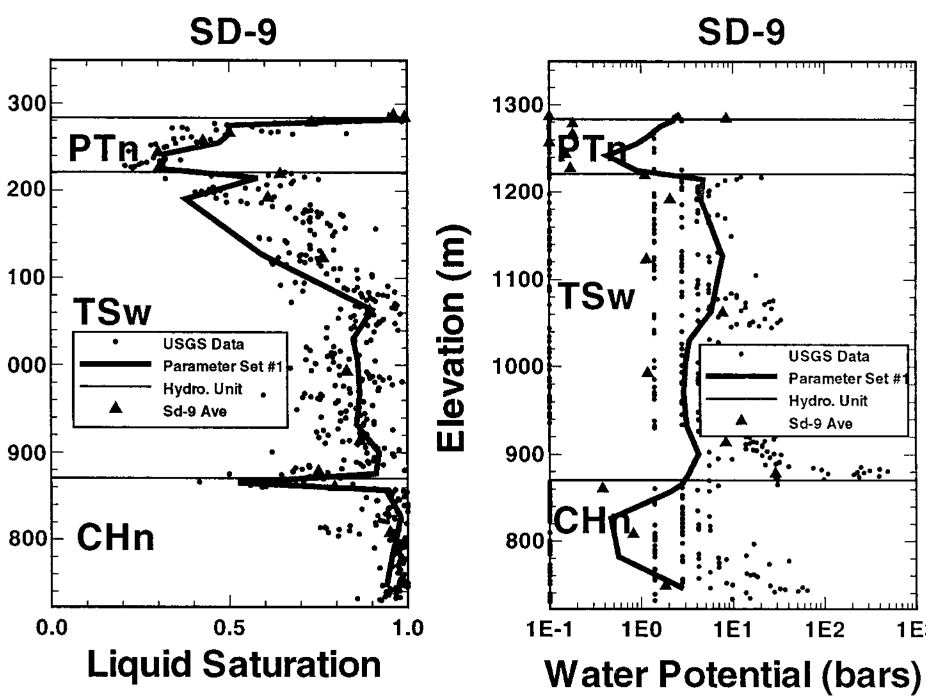

Fig. 7. Comparisons of the simulated and observed saturations and water potentials of borehole SD-9.

of soil retention curves; ϕ_f and $F\phi_f$ are porosities and fracture frequencies for fractures, respectively.

The properties for faults are listed in Table 3. There are four vertical zones for fault rock properties, i.e., each of the faults is subdivided into four hydrogeological units, TCw, PTn, TSw and CHn. The fracture and matrix properties for fault zones are derived based on pneumatic data analysis of the fault permeability (Ahlers et al., 1996), observed fracture distribution from underground tunnels (Sonnenthal et al., 1997), and previous studies (Ahlers et al., 1995a,b; Wittwer et al., 1995).

3. Model verification and calibration

As a critical step in developing the 3D UZ flow model, borehole-measured saturation, water potential and temperature data were compared with the model predictions. This is part of the important iterative processes of model calibration and verification to increase confidence in model predictions of the site condition. Liquid saturation data taken from five boreholes (OCRWM, DOE, 1995) were selected for the comparisons because the data were collected under an approved quality assurance program. Temperature data

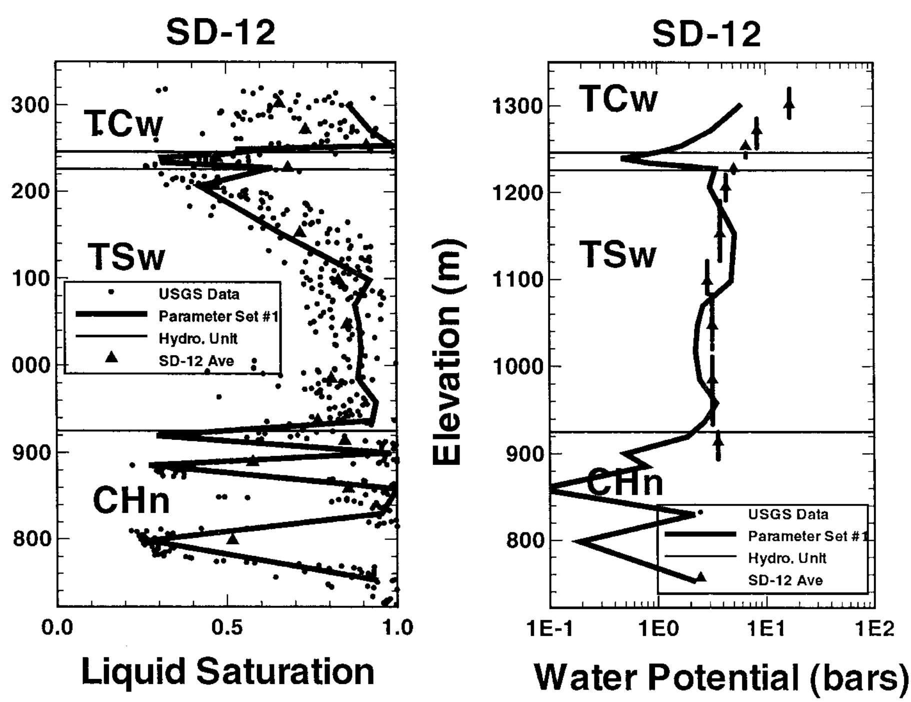

Fig. 8. Comparisons of the simulated and observed saturations and water potentials of borehole SD-12.

used for the study were selected from 25 boreholes as measured by Sass et al. (1988) and Rousseau (1996). These field-measured moisture and temperature data have been used in this study for analyzing effects of rock property variations, and for comparison between model simulations and observations. Simulations were conducted using combinations of parameters (Tables 2 and 3) and areally distributed infiltration rates (Fig. 3), and the boundary conditions discussed above.

The results of the steady-state TOUGH2 simulations were used in the following model verification study, and this implies that ambient moisture flow at Yucca Mountain is assumed to be at steady-state. A sampling of simulation results compared with field observations is presented in the following sections. The moisture flow calibrations were conducted using the dual-permeability model, whereas temperature studies were based on the ECM modeling approach to reduce the intensity of computational requirements when a dual-permeability were used. Many more model calibrations than those shown in this section were conducted to examine the capability of the site-scale model in predicting the ambient hydrological conditions. It has been found during these studies that in general a 3D model has to be used, instead of 1D or 2D models, in order to match the observation data. This is due to the three-dimensional nature of the mountain

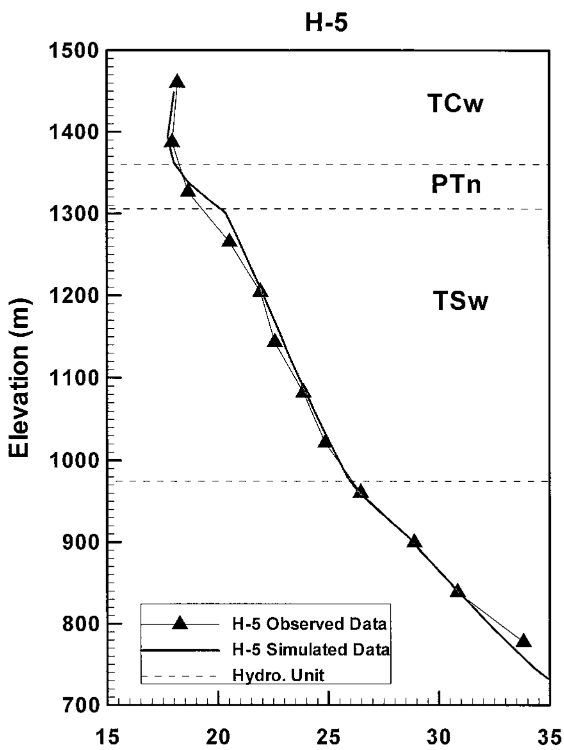

Fig. 9. Comparison between measured and simulated temperatures for borehole H-5.

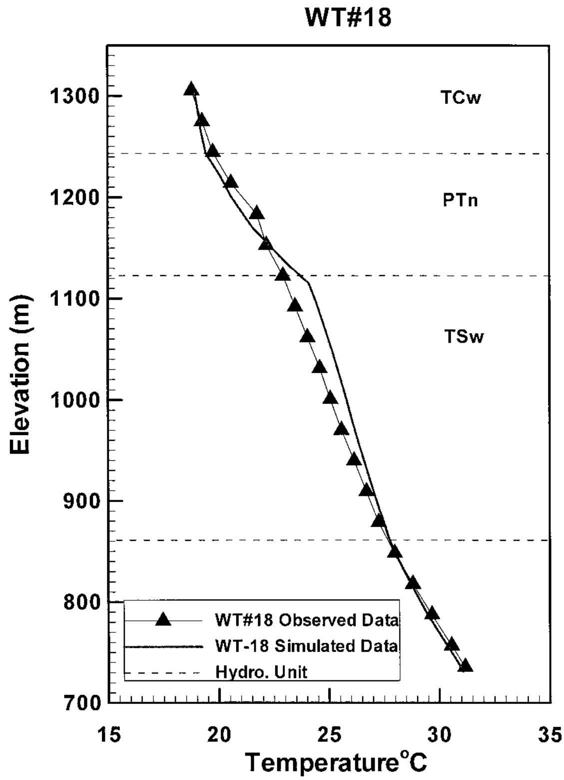

Fig. 10. Comparison between measured and simulated temperatures for borehole WT#18.

system in terms of fluid and heat flow and distributions, as well as the geological structure.

3.1. Comparisons of liquid saturations and water potentials

Simulated liquid saturation and water potential profiles were compared against observed profiles at the five boreholes UZ-14, UZ#16, SD-7, SD-9 and SD-12 (Figs. 4–8). In these figures, the simulated saturation profiles were extracted from the 3D simulations, while the borehole data are from field measurements. As shown in these figures, the simulated saturations are generally in good agreement with the measured saturation profiles at all the five locations for the four units (TCw, PTn, TSw, and CHn). In particular, the triangle data points (labeled as 'Ave') in these figures, which are calibration points for both 1D and 3D simulations, are matched well by the modeling results. Although comparisons with averaged water potential data are reasonable, they

---

Fig. 11. Simulated ambient saturations at the repository horizon and below in the UZ of Yucca Mountain, Nevada.

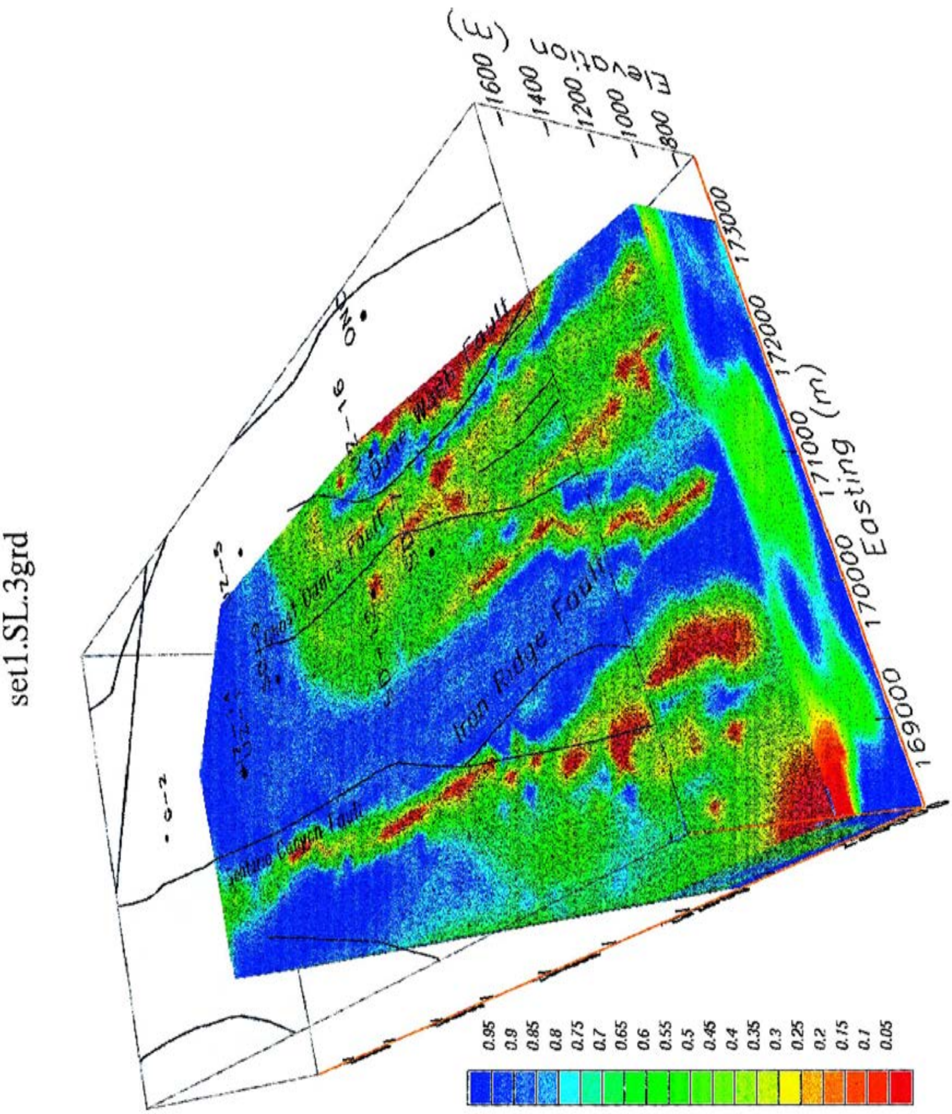
set1.SL.3grd
Elevation (m)
1600
1400
1200
1000
800
Easting (m)
169000
170000
171000
172000
173000
Iron Ridge Fault
Ghost Dance Fault
Dune Wash Fault
0.95
0.9
0.85
0.8
0.75
0.7
0.65
0.6
0.55
0.5
0.45
0.4
0.35
0.3
0.25
0.2
0.15
0.1
0.05

are not as good as the saturation profile matches. The reason for the poorer water potential comparisons may be due to inaccuracy in the measurement of these water potential data, both in terms of core measurements and in situ measurements.

3.2. Comparisons with temperature profiles

Measured temperature data (Sass et al., 1988; Rousseau, 1996) were compared with the 3D simulation results for 25 boreholes within and near the study area. The tabulated data in the Reference Information Base (RIB) (DOE, 1993), and the thermal data base (Brodsky et al., 1997) were used for rock thermal conductivities. In general, temperature data from the 25 boreholes matched reasonably well with the 3D model (Bodvarsson et al., 1997; Ahlers et al., 1995a). We present only two of the 25 comparisons conducted in the model calibration as demonstration examples. The selected boreholes are H-5 and WT#18, the locations of which are shown in Fig. 1.

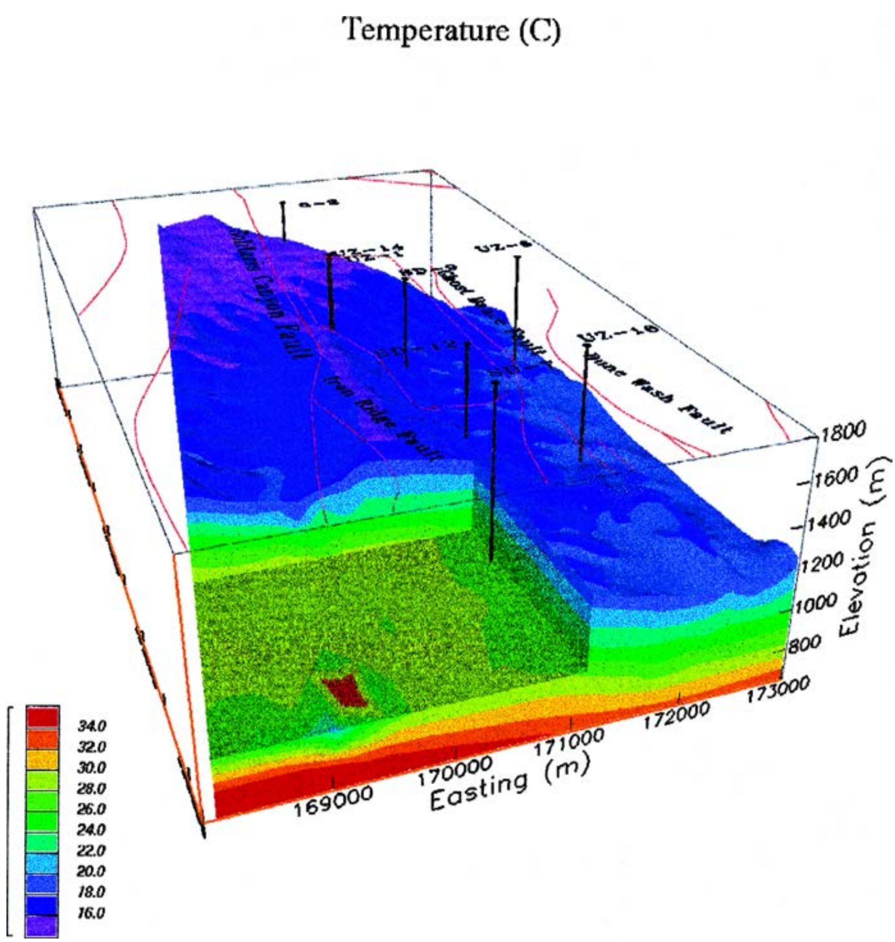

Fig. 12. Simulated ambient temperatures in the UZ of Yucca Mountain, Nevada.

The simulated temperature profiles are plotted in Figs. 9 and 10. The simulated temperature profiles match the data very well, as was the case for all the other borehole data / simulation comparisons.

4. Model predictions and discussions

This section demonstrates applications of the 3D UZ model to understanding moisture and heat flow at Yucca Mountain. We present simulation results and predictions to illustrate the effects of different rock properties and model conditions on the distribution and movement of moisture and heat within the mountain.

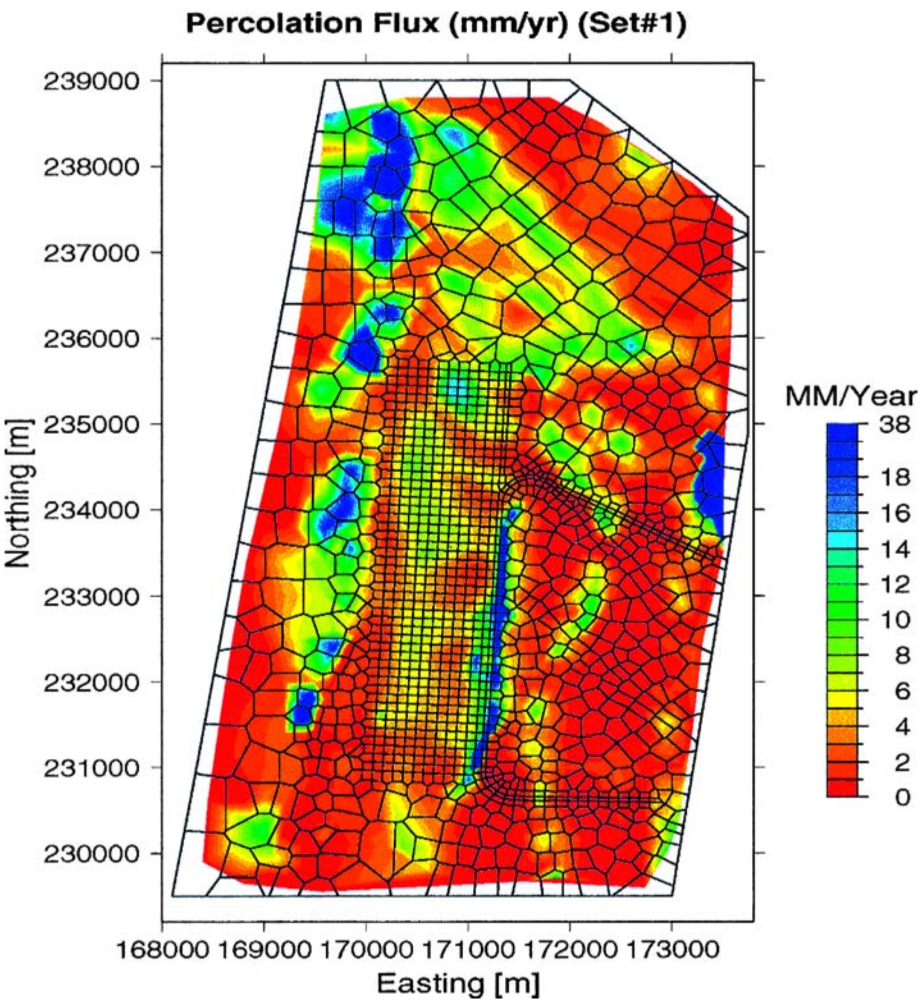

Fig. 13. Simulated percolation fluxes at repository horizon.

4.1. Ambient condition

The distribution and movement of moisture and heat within the mountain can be illustrated most effectively using 3D plots. Shown in Fig. 11 is a simulated 3D saturation plot, displaying liquid saturation distributions at and below the repository level. Fig. 11 indicates nonuniform distributions of liquid saturations at the repository horizon, with drier conditions prevailing along the faults and higher saturations away from these structures. The average saturations simulated at the repository level range from 0.8 to 0.9.

The simulated temperature distribution within the mountain is shown in Fig. 12. As can be seen in the figure, temperatures are at about 25°C at the repository level.

4.2. Percolation fluxes at repository horizon

Percolation flux through the UZ is one of the most critical factors considered in assessment of the repository performance. The quantity and spatial and temporal variations in percolation flux directly affect: (1) the quantity of water flowing into drifts;

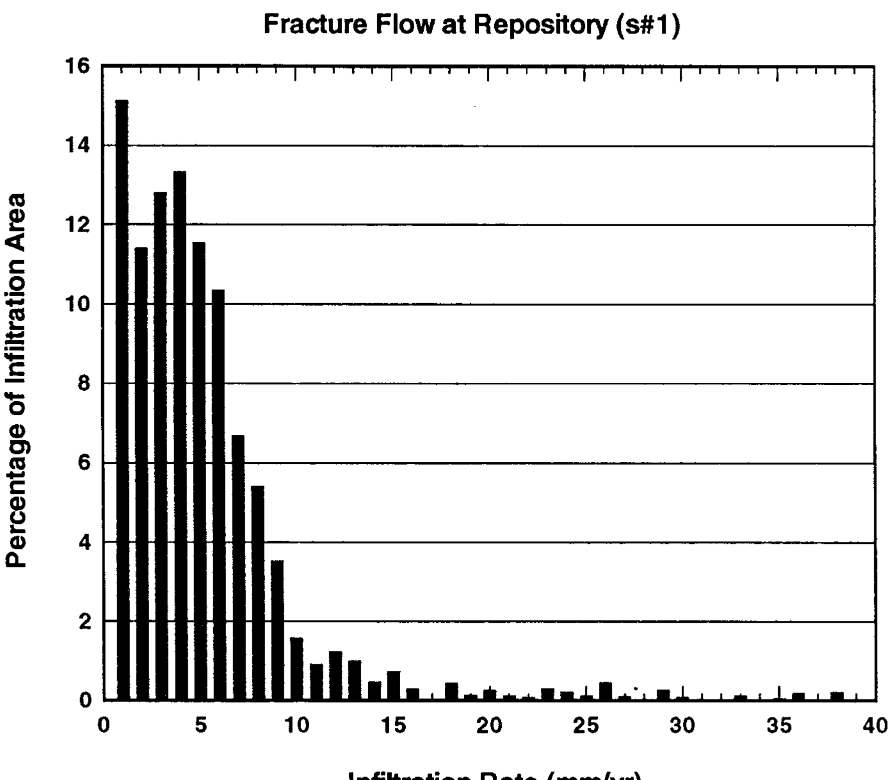

Fig. 14. Areal frequency and distribution of percolation fluxes within the repository area.

(2) moisture conditions and corrosion environment of canisters within the drifts; (3) waste mobilization from the repository; and (4) radionuclide migration to the saturated zone. However, percolation fluxes cannot be readily measured in the field, so one must rely on indirect data and model results to estimate them. Thus, one of the primary objectives of developing the UZ flow model is to provide a modeling analysis of percolation fluxes at the repository level.

The simulated percolation fluxes at the repository horizon are shown in Fig. 13, with statistics of flux distribution. Fracture and matrix flow components are given in Figs. 14–16. The percolation flux is defined in the figures as total mass flux through both fractures and matrix. Percolation fluxes are converted to millimeter per year (mm/year) per unit horizontal area for comparison with the commonly used infiltration rate unit.

Fig. 13 shows a nonuniform flux pattern of distributions, where the dark blue indicate higher percolation fluxes, or preferential flow pathways at the repository horizon. The higher percolation fluxes are mainly located at the northern part of model domain, and along the eastern boundary of the repository near the Ghost Dance fault. Comparison of the infiltration map of Fig. 3 and the simulated flux map of Fig. 13 indicates that flow is diverted laterally 500 m or more to the east between the ground surface and the repository level at the repository areas. The Ghost Dance fault is acting as a capillary

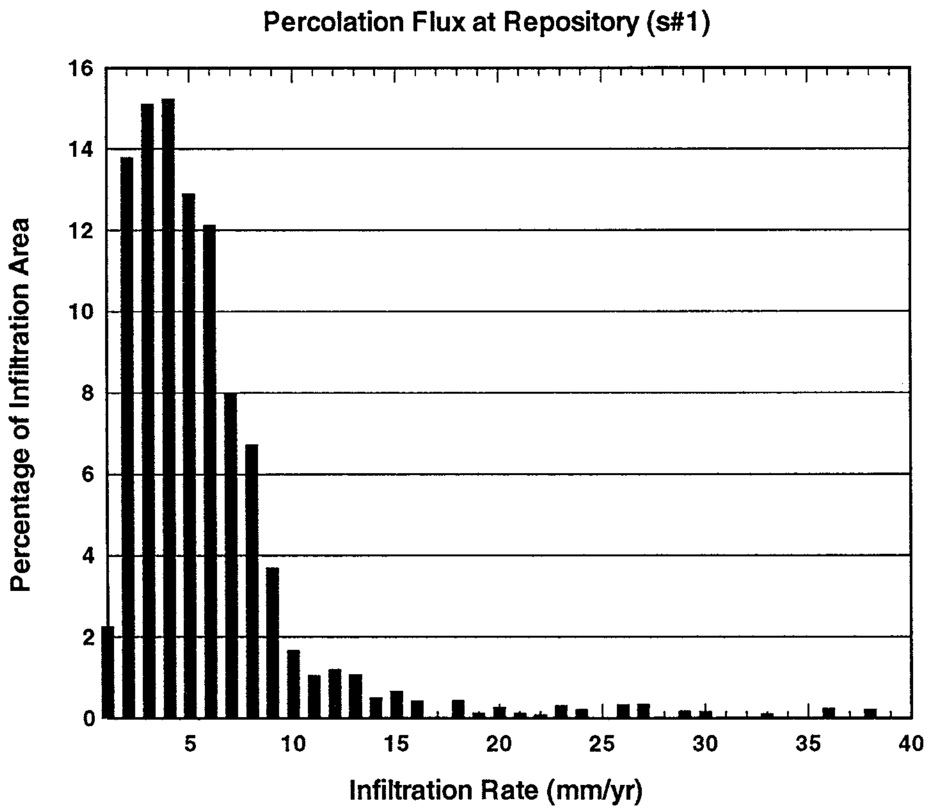

Fig. 15. Areal frequency and distribution of fracture fluxes within the repository area.

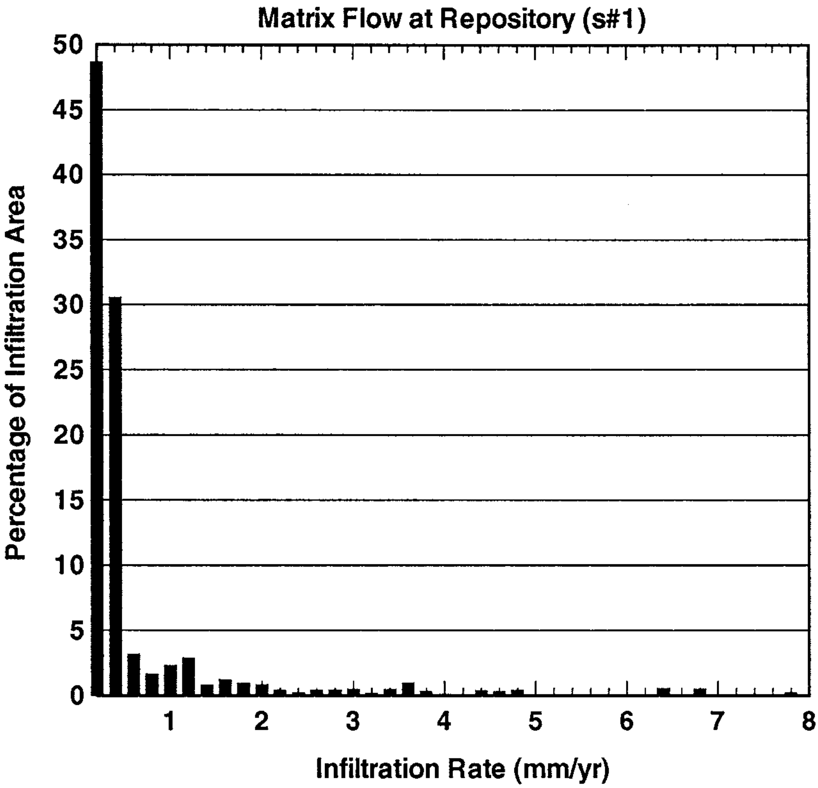

Fig. 16. Areal frequency and distribution of matrix fluxes within the repository area.

barrier in this simulation, creating a zone of high saturation along its west side. The average percolation flux simulated over the repository is about 5.5 mm/year, lower than the average value of 6.7 mm/year of surface infiltration rate over the repository area.

Fig. 14 shows a frequency distribution of percolation flux at the repository. The frequencies are generated by grouping the vertical flux results for the repository model nodal areas, counting the totals found in each group, and calculating the percent contribution relative to the total repository area in each category. On the plots, a node in the 1 mm/year category has a flux rate in the 0.0 to 1.0 mm/year range. Fig. 14 indicates that the highest flux frequencies, over about 30% of the repository area, have fluxes within the 2.0 to 4.0 mm/year range. The nodal area with percolation fluxes greater than 20.0 mm/year comprise only about 1% of the total repository area. 70% of the repository areas are estimated to have percolation fluxes between 1–6 mm/year.

Figs. 15 and 16 show the frequency and distribution of fracture and matrix flow over the repository area, respectively. Fig. 15 indicates the highest frequency of fracture flow within the repository is at the lowest flux range of 1 mm/year or less, which occurs over 15% of the repository area. Average fracture flow over the repository area is about 4–5 mm/year. Matrix flow at the proposed repository horizon (Fig. 16) is much lower, consistent with the densely welded nature of the units. More than 80% of matrix flow at the level of the repository takes place at rates of less than 1 mm/year. As shown by Figs. 15 and 16, the percentage of fracture flow is about 80% of the total flow at the level of the proposed repository. This indicates that fracture flow is the dominated flow mechanism at the repository level, because of low values of matrix permeability.

5. Concluding remarks

A 3D, site-scale unsaturated-zone model was developed for simulating moisture and heat flow at Yucca mountain. A systematic study of model verification, calibration and application was presented in this paper. The model verification and calibration efforts were performed using field data on moisture saturation, water potentials, and temperatures. The moisture and temperature distributions predicted by the 3D model match with observed water saturation, water potentials and temperature profiles. The model predicted that percolation fluxes at the repository horizon are very nonuniformly distributed, and they are affected by surface infiltration rates, heterogeneity of rock properties, and faults.

The development of the 3D model and the methodology used in the model calibrations presented in this paper constitute an important step in understanding fluid and heat flow within Yucca Mountain. This study provides confidence that the 3D site-scale unsaturated-zone model can incorporate all available field observations; however, there are still considerable uncertainties in our understanding of the entire hydrogeological system of Yucca Mountain. This is especially true with respect to the critical areas including fracture–matrix properties, present-day and future infiltration rates over the mountain, and conceptual models of fracture–matrix interactions. Future studies will be needed to more fully understand these phenomena.

In order to reduce the uncertainties associated with UZ flow and transport analyses, it is necessary to continue the UZ model calibration efforts incorporating all the updated field data, once they become available. The 3D model calibrations and sensitivity analysis reported in this paper are part of the continuous efforts to simulate and evaluate fluid flow and patterns within Yucca Mountain.

Acknowledgements

The authors are grateful to the two reviewers, Ning Lu and Sabodh Garg, for their critical review and constructive suggestions for improvement of this manuscript. Thanks are due to R.W. Zimmerman, J. Fairley, H.H. Liu and K. Huang for their careful review of this paper. Thanks are also due to A. Ritcey for her help in preparing this manuscript. This work was supported by the Director, Office of Civilian Radioactive Waste Management, US Department of Energy, through Memorandum Purchase Order EA9013MC5X between TRW Environmental Safety Systems and the Ernest Orlando

Lawrence Berkeley National Laboratory (Berkeley Lab). The support is provided to Berkeley Lab through the US Department of Energy Contract No. DE-AC03-76SF00098.

References

Ahlers, C.F., Bandurraga, T.M., Bodvarsson, G.S., Chen, G., Finsterle, S., Wu, Y.S., 1995. Summary of model calibration and sensitivity studies using the LBNL/USGS three-dimensional unsaturated zone site-scale model. Yucca Mountain Site Characterization Project Report.

Ahlers, C.F., Bandurraga, T.M.. Bodvarsson, G.S., Chen, G., Finsterle, S., Wu, Y.S., 1995. Performance analysis of the LBNL/USGS three-dimensional unsaturated zone site-scale model. Yucca Mountain Project Milestone 3GLM105M, Lawrence Berkeley National Laboratory, Berkeley, CA.

Ahlers, C.F., Shan, C., Haukwa, C., Cohen, A.B.J., Bodvarsson, G.S., 1996. Calibration and prediction of pneumatic response of at Yucca Mountain, Nevada using the unsaturated zone flow model. Yucca Mountain Project Milestone OB12M.

Ahlers, C.F. et al., 1998. Characterization and prediction of subsurface pneumatic response of at Yucca Mountain, Nevada, this issue.

Arnold, B.W., Altman, S.J., Robey, T.H., Barnard, R.W., Brown, T.J., 1995. Unsaturated-zone fast-path flow calculations for Yucca Mountain groundwater travel time analyses (GWTT-94). Yucca Mountain Site Characterization Project Report, SAND95-0857, UC-814.

Bandurraga, T.M., 1996. Vertical layering scheme for the numerical grid. In: Bodvarsson, G.S., Bandurraga, M. (Eds.), Development and Calibration of the Three-Dimensional Site-Scale Unsaturated-Zone Model of Yucca Mountain, Chap. 2. Nevada Yucca Mountain Site Characterization Project Report, Lawrence Berkeley National Laboratory, Berkeley, CA.

Bandurraga, T.M., Bodvarsson, G.S., 1997. Calibrating matrix and fracture properties using inverse modeling. In: Bodvarsson, G.S., Bandurraga, M., Wu Y.S. (Eds.), The Site-Scale Unsaturated Zone Model of Yucca Mountain, Nevada, for the Viability Assessment, Chap. 6. Yucca Mountain Site Characterization Project Report, LBNL-40376, UC-814, Lawrence Berkeley National Laboratory, Berkeley, CA.

Bandurraga, T.M., Finsterle, S., Bodvarsson, G.S., 1996. Saturation and capillary pressure analysis. In: Bodvarsson, G.S., Bandurraga, M. (Eds.), Development and Calibration of the Three-dimensional Site-Scale Unsaturated-Zone Model of Yucca Mountain, Nevada, Chap. 3. Yucca Mountain Site Characterization Project Report, Lawrence Berkeley National Laboratory, Berkeley, CA.

Bandurraga, T.M. et al., 1999. Calibrating Hydrogeologic Properties for the 3D Site-Scale Unsaturated Zone Model of Yucca Mountain, Nevada. J. Contam. Hydrol. 38, 25–46.

Bodvarsson, G.S., Shan, C., Htay, A., Ritcey, A., Wu, Y.S., 1997. Yucca estimation of percolation fluxes from temperature data. In: Bodvarsson, G.S., Bandurraga, M., Wu, Y.S. (Eds.), The Site-Scale Unsaturated Zone Model of Yucca Mountain, Nevada, for the Viability Assessment, Chap. 11. Mountain Site Characterization Project Report, LBNL-40376, UC-814, Lawrence Berkeley National Laboratory, Berkeley, CA.

Bodvarsson, G.S., Boyle, W., Hayes, L., Hoxie, D., Patterson, R., Williams, D., this issue. Overvew of scientific investigations at Yucca Mountain—The potentail repository for high-level nuclear waste.

Brodsky, N.S., Riggins, M., Connolly, J., Ricci, P., 1997. Thermal expansion, thermal conductivity, and heat capacity measurements for boreholes UE25 NRG-4, UE25 NRG-5, USW NRG-6, and USW NRG-7/7a. SAND 95-1955, Sandia National Laboratories, Albuquerque, NM, in press.

Buesch, D.C., Spengler, R.W., Moyer, T.C., Geslin, J.K., 1995. Nomenclature and macroscopic identification of lithostratigraphic units of the Paintbrush Group exposed at Yucca Mountain, Nevada. Report USGS OFR 94-469, U.S. Geological Survey.

DOE, 1993. Reference Information Base (RIB), Yucca Mountain Site Characterization Project.

Doughty, C., Bodvarsson, G.S., 1996. Investigation of conceptual and numerical approaches for evaluating gas, moisture, heat, and chemical transport. In: Bodvarsoon, G.S., Bandurraga, M. (Eds.), Development and Calibration of the Three-Dimensional Site-Scale Unsaturated-Zone Model of Yucca Mountain, Nevada, Chap. 6. Yucca Mountain Site Characterization Project Report, Lawrence Berkeley National Laboratory, Berkeley, California.

Doughty, C., Bodvarsson, G.S., 1997. Investigation of conceptual and numerical approaches for evaluating moisture flow and chemical transport. In: Bodvarsson, G.S., Bandurraga, M., Wu, Y.S. (Eds.), The Site-Scale Unsaturated Zone Model of Yucca Mountain, Nevada, for the Viability Assessment, Chap. 5. Yucca Mountain Site Characterization Project Report, LBNL-40376, UC-814, Lawrence Berkeley National Laboratory, Berkeley, CA.

Doughty, C., Bodvarsson, G.S., 1999. Investigation of conceptual and numerical approaches for evaluating moisture, gas, chemical, and heat transport in fractured unsaturated rock. J. Contam. Hydrol. 38, 69–106.

Flint, A.L., Flint, L.E., 1994. Spatial distribution of potential near surface moisture flux at Yucca Mountain, Nevada. Proceedings of the Fifth Annual International Conference on High Level Radioactive Waste Management, Las Vegas, Nevada, pp. 2352–2358.

Flint, A.L., Flint, L.E., Hevesi, J.A., 1993. The influence of long term climate change on net infiltration at Yucca Mountain, Nevada. Proceedings of the Fourth Annual International Conference on High Level Radioactive Waste Management, Las Vegas, Nevada, Vol. 1, pp. 152–159.

Flint, A.L., Hevesi, J.A., Flint, E.L., 1996. Conceptual and numerical model of infiltration for the Yucca Mountain Area, Nevada. U.S. Geological Survey, Water-Resources Investigation Report-96, Denver, Colorado.

Fridrich, C.J., DudleyJr, W.W., Stuckless, J.S., 1994. Hydrogeologic analysis of the saturated-zone ground water system, under Yucca Mountain, Nevada. J. Hydrol. 154, 133–168.

Ho, C.K., 1994. Modeling infiltration into a tuff matrix from a saturated vertical fracture. Proceedings of the Fifth Annual International Conference High Level Radioactive Waste Management, Sponsored by the American Nuclear Society and American Society of Civil Engineers, Las Vegas, Nevada, May 22–26, pp. 1897–1904.

Hudson, D.B., Flint, A.L., 1995. Estimation of Shallow Infiltration and Presence of Potential Fast Pathways for Shallow Infiltration in the Yucca Mountain Area, Nevada. USGS.

International Formulation Committee, 1967. A Formulation of the Thermodynamic Properties of Ordinary Water Substance. IFC Secretariat, Düsseldorf, Germany.

Lu, N., Kwicklis, E.M., 1995. A preliminary, two-dimensional numerical model for gas circulation around UZ6s, Yucca Mountain, Nevada. U.S. Geological Survey, Lakewood, CO.

Montazer, P., Wilson, W.E., 1984. Conceptual hydrologic model of flow in the unsaturated zone, Yucca Mountain, Nevada. Water Resources Investigations Report 84-4345, U.S. Geological Survey.

Narasimhan, T.N., Witherspoon, P.A., 1976. An integrated finite difference method for analyzing fluid flow in porous media. Water Resources Res. 12 (1), 57–64.

OCRWM, DOE, 1995. Technical Data Catalog, Yucca Mountain Site Characterization Project.

Pollock, D.W., 1986. Simulation of fluid flow and energy transport processes associated with high-level radioactive waste disposal in unsaturated alluvium. Water Resources Res. 22 (5), 765–775.

Pruess, K., 1991. TOUGH2—a general-purpose numerical simulator for multiphase fluid and heat flow. Report No. LBL-29400, Lawrence Berkeley Laboratory, Berkeley, CA.

Pruess, K., Narasimhan, T.N., 1985. A practical method for modeling fluid and heat flow in fractured porous media. Soc. Pet. Eng. J. 25, 14–26.

Pruess, K., Wang, J.S.Y., Tsang, Y.W., 1990a. On thermohydrologic conditions near high level nuclear wastes emplaced in partially saturated fractured tuff: Part 1. Simulation studies with explicit consideration of fracture effects. Water Resources Res. 26 (6), 1235–1248.

Pruess, K., Wang, J.S.Y., Tsang, Y.W., 1990b. On the thermohydrologic conditions near high-level nuclear wastes emplaced in partially saturated fractured tuff: Part 2. Effective continuum approximation. Water Resources Res. 26 (6), 1249–1261.

Pruess, K., Faybishenko, B., Bodvarsson, G.S., 1999. Alternative concepts and approaches for modeling flow and transport in thick unsaturated zones of fractured rocks. J. Contam. Hydrol. 38, 281–322.

Robinson, B.A., Wolfsberg, A.V., Zyvoloski, G.A., Gable, C.W., 1995. An unsaturated zone flow and transport model of Yucca Mountain. LANL-Milestone Report 3468.

Robinson B.A., Wolfsberg, A.V., Viswanathan, H.S., Zyvoloski, G.A., Gable, C.W., Turin, H.J., 1996. Modeling of flow, radionuclide migration, and environmental isotope distributions at Yucca Mountain. LANL-Milestone Report 3672.

Robinson, B.A., Wolfsberg, A.V., Gable, C.W., Krogh, K.C., Bower, K.M., Zyvoloski, G.A., Szarnecki, J.B.,

1997. Interm UZ and SZ transport model for PA abstraction/sensitivity analysis. LANL-Milestone Report SP342HM4.

Rockhold, M.L., Sagar, B., Connelly, M.P., 1990. Multi-dimensional modeling of unsaturated flow in the vicinity of exploratory shafts and fault zones at Yucca Mountain, Nevada. Proceedings of the First International Conference on High Level Radioactive Waste Management, Las Vegas, NV, pp. 1192–1199.

Rousseau, J.P., 1996. Data transmittal of pneumatic pressure records from 10/24/1994 through 3/31/1996 for boreholes UE-25 UZ#5, USW NRG-6, USW NRG-7a, USW SD-12, and USW UZ-7a, Yucca Mountain, Nevada. U.S. Geological Survey.

Rousseau J.P., Kwicklis, E.M., Gillies, C. (Eds.), 1996. Hydrogeology of the unsaturated zone, North Ramp area of the Exploratory Studies Facility, Yucca Mountain, Nevada. U.S. Geological Survey, Water-Resources Investigations 98-4050, 1996 (in print).

Rulon, J., Bodvarsson, G.S., Montazer, P., 1986. Preliminary numerical simulations of groundwater flow in the unsaturated zone, Yucca Mountain, Nevada. Report LBL-20553, Lawrence Berkeley National Laboratory, Berkeley, CA.

Sass, J.H., Lachenbruch, A.H., Dudley W.W., Jr., Priest, S.S., Munroe, R.J., 1988. Temperature, thermal conductivity, and heat flow near Yucca Mountain, Nevada: some tectonic and hydrologic implications. USGS OFR-87-649.

Scott, R.B., Bonk, J., 1984. Preliminary geologic map of Yucca Mountain, Nye County, Nevada, with geologic sections. Report USGS OFR-84-494, U.S. Geological Survey.

Sonnenthal, E.L., Ahlers, C.F., Bodvarsson, G.S., 1997. Fracture and fault properties for the UZ site-scale flow model. In: Bodvarsson, G.S., Bandurraga, M., Wu, Y.S., (Eds.), The Site-Scale Unsaturated Zone Model of Yucca Mountain, Nevada, for the Viability Assessment, Chap. 7. Yucca Mountain Site Characterization Project Report, LBNL-40376, UC-814, Lawrence Berkeley National Laboratory, Berkeley, CA.

Spengler R.W., Braun, C.A., Linden, R.M., Martin, L.G., Ross-Brown, D.M., Blackburn, R.L. 1993. Structural character of the Ghost Dance Fault, Yucca Mountain, Nevada. Proceedings of the Fourth Annual International Conference on High Level Radioactive Waste Management, Sponsored by the American Nuclear Society and American Society of Civil Engineers, Las Vegas, Nevada, April 26–30, pp. 653–659.

Tsang, Y.W., Pruess, K., 1987. A study of thermally induced convection near a high-level nuclear waste repository in partially saturated fracture tuff. Water Resources Res. 23 (10), 1958–1966.

van Genuchten, M., 1980. A closed form solution for predicting the properties the hydraulic conductivity of unsaturated soils. Soil. Sci. Soc. Am. J. 44, 892–898.

Wang, J.S.Y., Narasimhan, T.N., 1985. Hydrologic mechanisms governing fluid flow in partially saturated, fractured, porous tuff at Yucca Mountain. Water Resources Res. 21, 1861–1874.

Wang, J.S.Y., Narasimhan, T.N., 1987. Hydrologic modeling of vertical and lateral movement of partially saturated fluid flow near a fault zone at Yucca Mountain. SAND87-7070, Sandia National Laboratories and LBL-23510, Lawrence Berkeley National Laboratory, Berkeley, CA.

Warren, J.E., Root, P.J., 1963. The behavior of naturally fractured reservoirs, Soc. Pet. Eng. J., pp. 245–255; Transactions, AIME, 228.

Weeks, E.P., 1987. Effects of topography on gas flow in unsaturated fractured rock: concepts and observations, flow and transport through unsaturated rock, In: Evens, D.D., Nicholson, T.J., (Eds.). Geophysical Monograph 42. American Geophysical, Union, Washington, DC, pp. 165–170.

Wittwer, C., Bodvarsson, G.S., Chornack M.P., Flint, A.L., Flint, L.E., Lewis, B.D., Spengler, R.W., Rautman, C.A., 1992. Design of a 3D site-scale model for the unsaturated zone at Yucca Mountain, Nevada. Proceedings of the Third International High-Level Radioactive Waste Management Conference, American Nuclear Society, pp. 263–71.

Wittwer, C., Chen, G., Bodvarsson, G.S., Chornack, M.P., Flint, A.L., Flint, L.E., Kwicklis, E., Spengler, R.W., 1995. Preliminary development of the LBL/USGS three-dimensional site-scale model of Yucca Mountain, Nevada. Report LBL-37356, UC-814, Lawrence Berkeley National Laboratory, Berkeley, CA.

Wu, Y.S., Pruess, K., 1988. A multiple-porosity method for simulation of naturally fractured petroleum reserviors. SPE Reservoir Eng. 3, 327–336.

Wu, Y.S., Chen, G., Bodvarsson, G.S., 1995. Preliminary analysis of effects of thermal loading on gas and heat flow within the framework of the LBNL/USGS site-scale model. Research Report LBL-37229, UC-814, Lawrence Berkeley National Laboratory, Berkeley, CA.

Wu, Y.S., Chen, G., Haukwa, C., Bodvarsson, G.S., 1996a. Three-dimensional model calibration and sensitivity studies. In: Bodvarsson, G.S., Bandurraga, M., (Eds.), Development and Calibration of the Three-Dimensional Site-Scale Unsaturated-Zone Model of Yucca Mountain, Nevada, Chap. 8. Yucca Mountain Site Characterization Project Report, Lawrence Berkeley National Laboratory, Berkeley, CA.

Wu, Y.S., Finsterle, S., Pruess, K., 1996b. Computer Models and their development for the unsaturated zone model at Yucca Mountain. In: Bodvarsson, G.S., Bandurraga, M. (Eds.), Development and Calibration of the Three-Dimensional Site-Scale Unsaturated-Zone Model of Yucca Mountain, Nevada, Chap. 4. Yucca Mountain Site Characterization Project Report, Lawrence Berkeley National Laboratory, Berkeley, CA.

Wu, Y.S., Ritcey, A.C., Haukwa, C., Bodvarsson, G.S., 1997. Integrated 3-D site-scale flow model: In: Bodvarsson, G.S., Bandurraga, M., Wu, Y.S. (Eds.), The Site-Scale Unsaturated Zone Model of Yucca Mountain, Nevada, for the Viability Assessment, Chap. 19. Yucca Mountain Site Characterization Project Report, LBNL-40376, UC-814, Lawrence Berkeley National Laboratory, Berkeley, CA.